Carbogenic nanoparticles

DOI: 10.1002/smll.200700578

Surface Functionalized Carbogenic Quantum Dots**

*Athanasios B. Bourlinos, Andreas Stassinopoulos, Demetrios Anglos, Radek Zboril, Michael Karakassides, and Emmanuel P. Giannelis**

Quantum dots are semiconductor nanocrystals that inherently fluoresce at specific wavelengths in the visible, enabling a number of potential applications to be realized.[1] However, conventional quantum dots are based on metallic elements, which has raised concerns over toxicity, stability and high cost. As a result, the search for more benign substitutes is a worthwhile yet challenging undertaking. Recently a new type of visible emitters has been reported exclusively based on functionalized carbon nanoparticles.[2] The carbon dots were 5 nm in diameter and were produced via laser ablation of graphite. Surface oxidation with nitric acid and subsequent covalent grafting of organic moieties afforded light-emitting derivatives. Notably, the light emitted by these dots depends on the wavelength of light used for excitation. It was suggested that the tethered modifier stabilizes the surface of the carbon nanoparticles helping to generate energy traps that emit light when stimulated, an effect described as emission from passivated surfaces. Because of its origin the emission is size-dependent, i.e., the smaller the size of the dots the better their photoluminescence efficiency.[2] In another intriguing approach, photoluminescent carbon dots 3 nm in size were directly fabricated by electrochemical shocking of multi-wall carbon nanotubes.[3] The demonstrated photoluminescence adds another dimension to the versatility of carbon-based materials and holds promise in the advancement of new nanocarbon emitters.[4]

Alternative synthetic approaches solely based on chemistry are desirable in order to achieve better control of the size, shape and physical properties of the carbon particles. Significant body of literature refers to the chemical synthesis of individual carbon nanoparticles. Nevertheless, the reported sizes typically range from 20 to 200 nm and seldom fall below 10 nm.[5] As such, no efficient emission has been observed for these systems in the visible. In addition, the as-obtained particles lack dispersibility in any solvent. Thus, a post surface treatment is necessary in order to obtain colloidal fluids. To that end, we report here an entirely different approach for synthesizing surface functionalized carbogenic nanoparticles via thermal carbonization of suitable molecular precursors. We refer to these particles as carbogenic because of their oxygen content. The nanoparticles produced via this one-step pyrolysis method are monodisperse with sizes less than 10 nm and they are in effect dispersible in various solvents depending on the nature of the surface modifier. Furthermore, the carbogenic nanoparticles reported here fluoresce in the visible, when stimulated with a wide range of excitation wavelengths. Two different chemical routes are discussed below. The first one is based on citrate and the other on 4-aminoantipyrine precursors, respectively. The choice of a particular carbon source partly depends on its ability to afford pyrolytic products that are practically insoluble in basic or acidic aqueous solutions.

In the first route, the capped nanoparticles are derived in a simple, one-step thermal decomposition of different ammonium citrate salts, where the citrate unit serves as the source of carbon[6] while the compensating organic ammonium provides the covalently attached surface modifier. Carbonization of the octadecyl ammonium ($C_{18}H_{37}NH_3^+$) citrate salt results in organophilic nanoparticles, whereas carbonization of the 2-(2-aminoethoxy)-ethanol ($OHCH_2CH_2OCH_2CH_2NH_3^+$) salt results in hydrophilic nanoparticles. In both cases, the resulting amide linkages[7] (–NHCO–) from the thermal dehydration of the ammonium carboxylate moieties ($–NH_3^{+-}OOC–$) tether the organic corona covalently to the cores. The low melting point of the specific citrate salts, which enables the growth of rather uniform nanoparticles from the liquid phase, as well as the surface blocking provided by the organic corona are believed to contribute to both monodispersity and ultrafine, nanoscale dimensions. Due to their organophilic or hydrophilic corona each particular derivative is readily dispersible at high concentrations (50 mg mL^{-1}) in organic (toluene, chloroform, tetrahydrofuran, hexane) or aqueous solvents, respectively. In contrast, pyrolysis of neat citric acid results in a completely insoluble carbogenic solid. It is worth noting that the carbogenic cores share a common stoichiometry with graphite oxide[8] (see Experimental Section). It is suggested that the cores consist of carbonized intermediates with a highly defected structure of co-existing aromatic and aliphatic regions, in analogy with graphite oxide or the interrelated carbogenic networks of lignite, coal and humic substances.[8,9] The highly fluorescent nature of the nanoparticles (see below) prevented further structural/chemical characterization using Raman spectroscopy.

[*] Prof. E. P. Giannelis
Department of Materials Science and Engineering, Cornell University
Ithaca, NY 14853 (USA)
E-mail: epg2@cornell.edu

Dr. A. B. Bourlinos
Institute of Materials Science, NCSR "Demokritos"
Ag. Paraskevi Attikis, Athens 15310 (Greece)

A. Stassinopoulos, Dr. D. Anglos
Institute of Electronic Structure and Laser
Foundation for Research and Technology-Hellas
P.O. Box 1385, GR-711 10 Heraklion, Crete (Greece)

Prof. R. Zboril
Department of Physical Chemistry, Palacky University
Olomouc 77146 (Czech Republic)

Prof. M. Karakassides
Department of Materials Science and Engineering
University of Ioannina
45110 Ioannina (Greece)

[**] E. P. G. acknowledges the support of CFCI funded by DOE. A. S. receives a graduate fellowship through project ΠΕΝΕΔ-contract 03ΕΔ581. R. Z. acknowledges the support by the Projects of the Ministry of Education of the Czech Republic (1M619895201 and MSM6198959218).

Supporting Information is available on the WWW under http://www.small-journal.org or from the author.

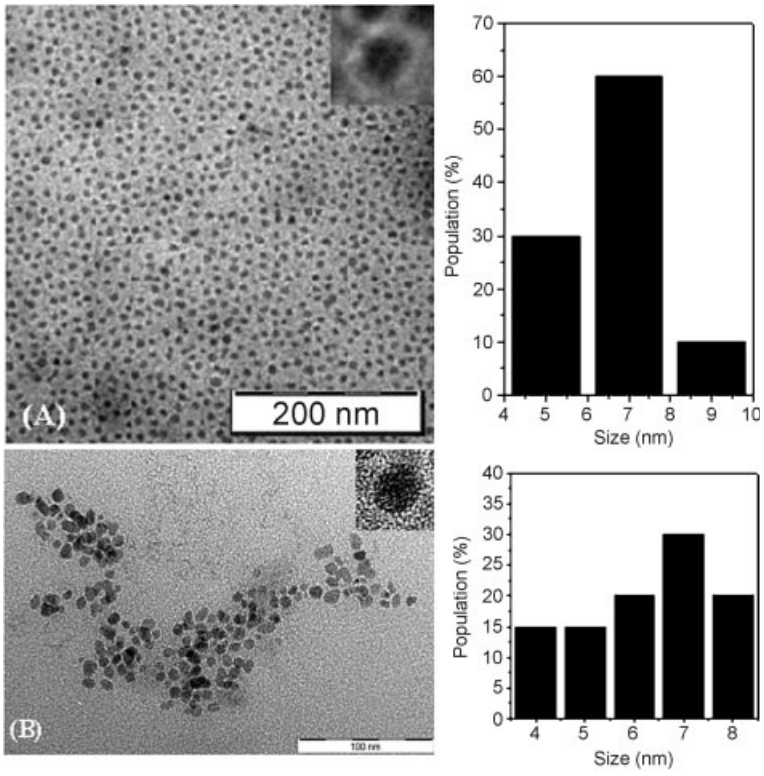

Figure 1. A) TEM image of the organophilic derivative. The inset shows an individual carbogenic nanoparticle with a hallo ring around its surface. B) TEM micrograph of the aqueous-dispersible nanoparticles. The inset shows in magnification a single nanoparticle. The corresponding size histograms are given aside.

The IR spectrum of the octadecyl-derivative (see Fig. S1 in the Supporting Information) shows characteristic absorption peaks due to the octadecyl chains tethered to the surface. In addition to these peaks, we also observe a strong, sharp peak at 1700 cm^{-1} suggestive of amide linkages. The corresponding XRD pattern (Fig. S1) displays two superimposed reflections: one broad centered at $d_{002} = 4.3$ Å attributed to highly disorder carbon[10] and another, sharper, at 4.14 Å typical for the inter-chain distance of densely packed alkyl chains.[11] Transmission electron microscopy (TEM) imaging (Fig. 1A) shows fairly monodisperse nanoparticles of near spherical morphology with an average size of 7 nm. In the inset the higher magnification image shows the corona molecules as a halo around the nanoparticles.

The IR spectrum of the hydrophilic derivative also exhibits the amide band as well as the characteristic absorptions of the corona molecules (see Fig. S2 in the Supporting Information). However, the hydrophilic nanoparticles seem to adopt a more amorphous structure than the organophilic analogue. The X-ray diffraction (XRD) pattern shows a broad peak centered at 0.5 nm (Fig. S2). TEM analysis (Fig. 1B) shows the formation of near spherical but less monodisperse nanoparticles with an average size of 7 nm. The distance between nanoparticles is markedly shorter than that in the organophilic derivative possibly due to the shorter length of the attached corona and possible hydrogen-bonding interactions among adjacent nanoparticles through the pending hydroxyl end-groups of the corona.

The absorption and emission spectra of the organophilic nanoparticles in CH_2Cl_2 (Fig. 2A) are comparable to those previously reported for functionalized carbon dots.[2,3] The emission band maximum shifts to longer wavelengths as the excitation wavelength increases across the whole visible range, a behavior that is also observed with the hydrophilic nanoparticles in water (Fig. 2B). We speculate that the ultrafine size of the dots combined with their disorder structure favor a high concentration of defect sites at the surface that give rise to the observed emission.[2] EPR probing of these defect sites revealed a narrow derivative signal of Lorentzian shape ($\Delta H_{pp} \sim 3.8$ G) centered at $g \sim 2.0042(2)$ (see Fig. S3 in the Supporting Information). This sharp line is characteristic of free radicals.[8] Besides this mechanism, the pyrolytic formation of several different fluorophores within the carbogenic network cannot be also ruled out.[12]

The fluorescence quantum yield of the hydrophilic particles measured against a methanol solution of rhodamine 6G (λ_{exc}: 495 nm) is about 3%, and virtually independent of the excitation wavelength in the 400–500 nm range. This behavior is different from that reported previously Sun et. al.[2] (i.e., quantum yield of 4–10% but wavelength-dependent) most likely due to different nanoparticles composition and structure as well as evaluation method. A detailed optical study is underway and will be presented in a forthcoming publication.

In the second route, the carbogenic dots (4AAP30) are derived by air-pyrolysis of 4-aminoantipyrine (4AAP) (Fig. 3). The wealth of 4-aminoantipyrine derivatives[13] sets the ground for the development of a wider series of carbogenic dots with desirable properties. According to TEM the carbogenic nanoparticles (5–9 nm) adopt a variety of shapes, ranging from near globular to rectangular. Although the particles appear strongly aggregated, they are highly dispersible (50 mg mL^{-1}) in DMSO, DMF and $CF_3CH(OH)CF_3$. Because of their high dispersability in solvents we suspect the particles are capped with an organic (possibly polymeric) corona. The nature of the corona is presently unknown, since there are no data in the literature describing in detail the polymerization of 4AAP. However, polymerization may occur through ring opening of the five-member ring of pyrazolinone or/and through the double bond.[14] We hypothesize that the first step of the synthesis comprises polymerization of the molecular precursor followed by partial carbonization of the resulting polymer. The polymeric corona on the surface of the nanoparticles controls their growth during pyrolysis. Note that similarly to the citrate salts, 4-aminoantipyrine is also a low-melting-point compound.

The IR spectrum of the molecular precursor is composed of characteristic –NHCO–, $–NH_2$, $–CH_3$ and $–C_6H_5$ absorption bands.[13a] After carbonization, the product still exhibits a broad absorption at 1630 cm^{-1} due to the amide band and

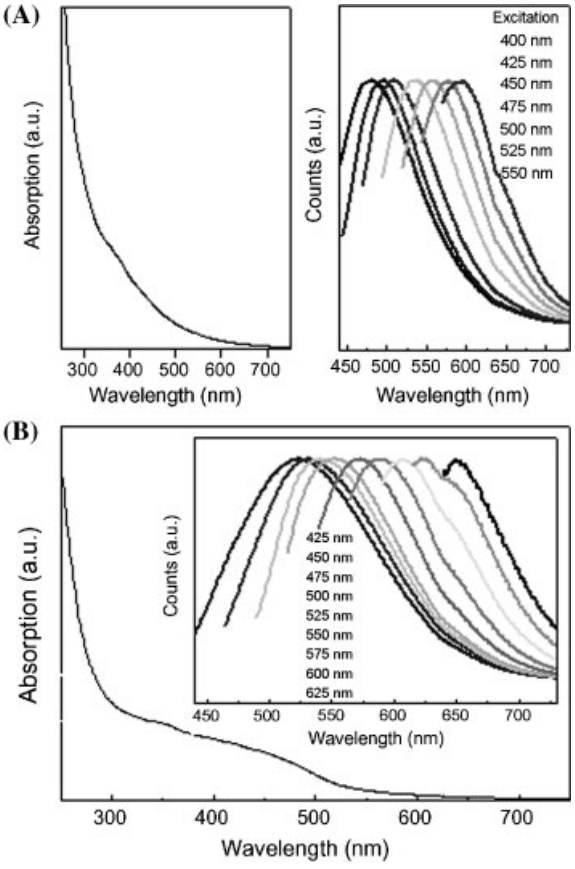

Figure 2. A) Left: absorption spectrum of the organophilic nanoparticles in CH_2Cl_2. Right: the corresponding normalized fluorescence spectra at different excitation wavelengths. B) Absorption spectrum of the hydrophilic nanoparticles in water. Inset: the corresponding normalized fluorescence spectra at different excitation wavelengths.

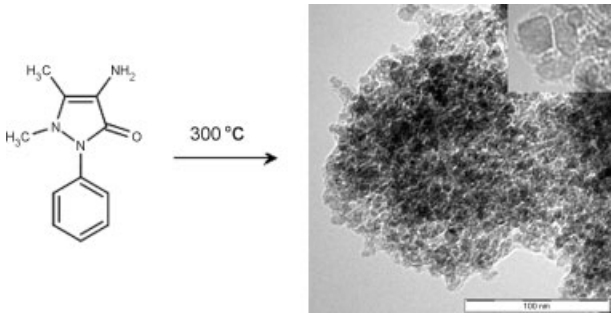

Figure 3. Synthesis scheme and TEM image for 4AAP30.

several other peaks due to remaining methyl and phenyl groups (see Fig. S4 in the Supporting Information). These bands are probably due to the polymeric corona on the particles. The XRD pattern of the crystalline precursor changes drastically after carbonization giving two superimposed broad reflections: one at 0.49 nm consistent with disorder carbon[10] and another at 0.35 nm implying the

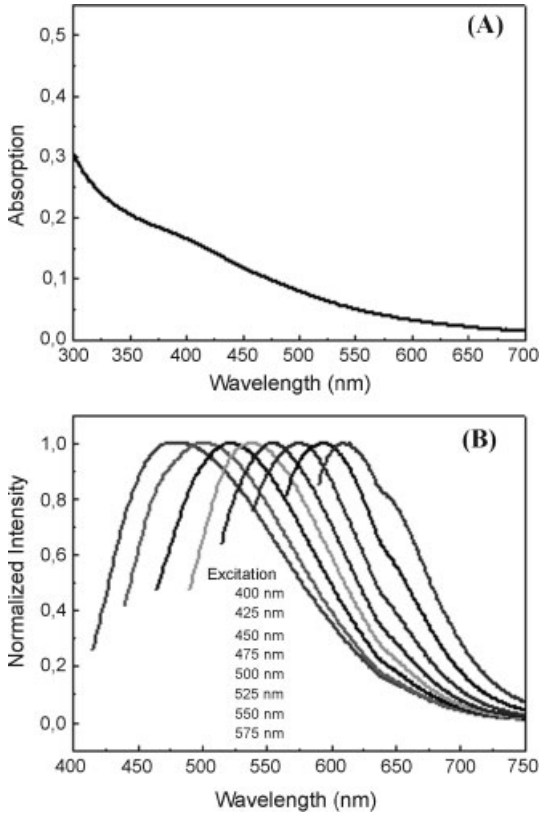

Figure 4. Absorption spectrum of 4AAP30 in DMF (A) and the corresponding normalized emission spectra at different excitation wavelengths (B).

presence of densely packed phenyls[15] within the polymeric corona (Fig. S4). Lastly, the absorption and emission spectra of 4AAP30 in DMF (Fig. 4) exhibit the same fluorescent behavior described for the carbogenic dots derived from the citrate salts.

In summary, we present a new approach to synthesize surface-functionalized carbogenic nanoparticles with unique optical features. The functionalized nanoparticles are obtained in a single step by thermal decomposition of either different ammonium citrate salts or 4-aminoantipyrine. The nanoparticles possess an average size of less than 10 nm, are highly dispersible in organic or aqueous solvents depending on their surface functionalization and emit light in the visible when stimulated with different excitation wavelengths.

Experimental Section

Citrate Route: For the organophilic nanoparticles, citric acid monohydrate (1.0 g, 4.8 mmol) was dissolved in ethanol (25 mL) followed by the addition of an ethanol solution containing $C_{18}H_{37}NH_2$ (Alfa Aesar, 1.5 g, 5.6 mmol). The mixture was stirred for 1 h and the precipitate formed was filtered, washed with ethanol and dried. The salt was then directly calcined in air at 300 °C for 2 h and a heating rate of 10 °C min^{-1}. The resulting solid was repeatedly washed with acetone and ethanol and dried (yield 10%).

Elemental analysis suggests an average chemical formula of: $(C_{18}H_{37}NH)(C_4O_{1.8})$. In the case of the hydrophilic nanoparticles, citric acid monohydrate (2 g, 9.5 mmol) was dissolved in water (10 mL) and $HOCH_2CH_2OCH_2CH_2NH_2$ (Aldrich, 1.3 g, 12.4 mmol) was added. The solution was evaporated until dry at 65 °C for 3 days and the resulting thick syrup was heated hydrothermally in a Teflon equipped stainless steel autoclave at 300 °C for 2 h and a heating rate of 10 °C min^{-1}. In this instance, the hydrothermal conditions were preferred over direct pyrolysis in air because of the ligand's higher sensitivity against degradation. The solid product was copiously washed with acetone leaving behind a residue that was then dispersed in water and filtered off. The hydrophilic derivative was obtained form the filtrate by water evaporation (yield 10%). Elemental analysis gives an average formula: $(OHCH_2CH_2OCH_2CH_2NH)(C_{4.3}O_{2.1}H_{0.4})$. Alumina TLC in toluene or water (single band, $R_f \sim 0$) and TGA (dec. > 300 °C) suggest the presence of pure materials void of any impurities or volatile byproducts.

4-Aminoantipyrine Route: 4-aminoantipyrine (4AAP, Aldrich, 2 g, 9.8 mmol) was directly calcined in air at 300 °C for 2 h at a heating rate of 10 °C min^{-1}. The as-derived carbogenic solid was dissolved in $CF_3CH(OH)CF_3$ (10 mL) and the deep brown clear colloid was precipitated by adding water (40 mL). The supernatant liquid was discarded and the precipitate was washed thoroughly with water, re-suspended in ethanol and centrifuged. Following several washings with ethanol the remaining solid was finally dried in air. The product denoted as 4AAP30 was obtained in 10% yield. Elemental analysis corresponds to the average formula: $C_{6.6}H_{6.1}N_{1.6}O$. ^{13}C NMR in d6-DMSO gave no detectable signals while the corresponding ^1H NMR spectrum exhibited broad signals of weak intensity mainly attributed to the methyl and phenyl groups present in the polymeric corona. Decomposition temperature: >300 °C (based on TGA).

Characterization: XRD patterns were recorded on a Siemens XD-500 diffractometer using CuKα radiation. The patterns were collected using background-free holders. IR spectra were made on an FT-IR spectrometer (Bruker Equinox 55/S) using KBr pellets. TEM was carried out on a JEOL JEM 2010 microscope operated at 200 kV (LaB6 cathode, point resolution 1.94 Å). For this study, few drops of a particular dilute dispersion were placed on a copper grid and evaporated prior to direct imaging. TGA traces were obtained with a Perkin-Elmer Pyris TGA/DTA instrument at a heating rate of 10 °C min^{-1}. EPR spectra were recorded in the solid state on a Bruker 200 D-SRC spectrometer equipped with an Anritsu microwave frequency counter. The absorption optical spectra were collected on a Cary 50 UV/Vis spectrophotometer (Varian), while fluorescence emission spectra were recorded on a Fluoromax-P fluorimeter (Jobin–Yvon). Elemental analysis (C, H, N) was performed using a Perkin Elmer 2400 analyzer.

Keywords:

carbogenic nanoparticles · carbonization · molecular precursors · photoluminescence · surface functionalization

[1] 1a) A. P. Alivisatos, *Science* **1996**, *271*, 933; b) A.P Alivisatos, *Nat. Biotechnol.* **2004**, *22*, 47.
[2] Y.-P. Sun, B. Zhou, Y. Lin, W. Wang, K. A. S. Fernando, P. Pathak, M. J. Meziani, B. A. Harruff, X. Wang, H. Wang, P. G. Luo, H. Yang, M. E. Kose, B. Chen, L. M. Veca, S.-Y. Xie, *J. Am. Chem. Soc.* **2006**, *128*, 7756.
[3] J. Zhou, C. Booker, R. Li, X. Zhou, T.-K. Sham, X. Sun, Z. Ding, *J. Am. Chem. Soc.* **2007**, *129*, 744.
[4] a) J. E. Riggs, Z. Guo, D. L. Carroll, Y.-P. Sun, *J. Am. Chem. Soc.* **2000**, *122*, 5879; b) Y. Sun, S. R. Wilson, D. I. Schuster, *J. Am. Chem. Soc.* **2001**, *123*, 5348; c) X. Xu, R. Ray, Y. Gu, H. J. Ploehn, L. Gearheart, K. Raker, W. A. Scrivens, *J. Am. Chem. Soc.* **2004**, *126*, 12736; d) F. Zhang, Y. Fang, *J. Phys. Chem. B* **2006**, *110*, 9022; e) Z. G. Wang, X. T. Zu, L. M. Fang, *J. Nanopart. Res.* **2007**, *9*, 289.
[5] a) X. Sun, Y. Li, *Angew. Chem.* **2004**, *116*, 607. *Angew. Chem. Int. Ed.* **2004**, *43*, 597; b) C. Tang, K. Qi, K. L. Wooley, K. Matyjaszewski, T. Kowalewski, *Angew. Chem.* **2004**, *116*, 2843. *Angew. Chem. Int. Ed.* **2004**, *43*, 2783; c) A. Yan, B. W. Lau, B. S. Weissman, I. Külaots, N. Y. C. Yang, A. B. Kane, R. H. Hurt, *Adv. Mater.* **2006**, *18*, 2373; d) A. B. Fuertes, P. Tartaj, *Small* **2007**, *3*, 275; e) L. Zhi, J. Wang, G. Cui, M. Kastler, B. Schmaltz, U. Kolb, U. Jonas, K. Müllen, *Adv. Mater.* **2007**, *19*, 1849.
[6] a) J. Moskon, R. Dominko, M. Gaberscek, R. Cerc-Korosec, J. Jamnik, *J. Electrochem. Soc.* **2006**, *153*, A1805; b) M. Gaberscek, R. Dominko, M. Bele, M. Remskar, J. Jamnik, *Solid State Ionics* **2006**, *177*, 3015.
[7] M. B. Smith, J. March, *March's Advanced Organic Chemistry: Reactions, Mechanisms, and Structure,* Wiley-Interscience, New York, 2001, p 508.
[8] T. Szabó, O. Berkesi, P. Forgó, K. Josepovits, Y. Sanakis, D. Petridis, I. Dékány, *Chem. Mater.* **2006**, *18*, 2740.
[9] a) A. Sakakibara, *Wood Sci. Technol.* **1980**, *14*, 89; b) D. G. Levine, R. H. Schlosberg, B. G. Silbernagel, *Proc. Natl. Acad. Sci. USA* **1982**, *79*, 3365; c) E. M. Peña-Méndez, J. Havel, J. Patočka, *J. Appl. Biomed.* **2005**, *3*, 13.
[10] a) Y. Liu, J. S. Xue, T. Zheng, J. R. Dahn, *Carbon* **1996**, *34*, 193; b) Y. Matsuo, Y. Sugie, *Carbon* **1998**, *36*, 301.
[11] A. B. Bourlinos, S. R. Chowdhury, D. D. Jiang, Y.-U. An, Q. Zhang, L. A. Archer, E. P. Giannelis, *Small* **2005**, *1*, 80.
[12] M. M. De Souza Sierra, O. F. X. Donard, M. Lamotte, C. Belin, M. Ewald, *Mar. Chem.* **1994**, *47*, 127.
[13] a) R. M. Issa, A. M. Khedr, H. F. Rizk, *Spectrochim. Acta Part A* **2005**, *62*, 621; b) O. Otim, *Int. J. Chem. Kinet.* **2001**, *33*, 600.
[14] a) N. Nemoto, X. Xu, F. Sanda, T. Endo, *Macromolecules* **2001**, *34*, 7642; b) I. Labádi, E. Pál, R. Tudose, O. Costisor, *J. Therm. Anal. Calorim.* **2006**, *83*, 681.
[15] K. Lee, S. Cho, S. H. Park, A. J. Heeger, C.-W. Lee, S.-H. Lee, *Nature* **2006**, *441*, 65.

Received: July 23, 2007
Revised: November 21, 2007
Published online: March 18, 2008

